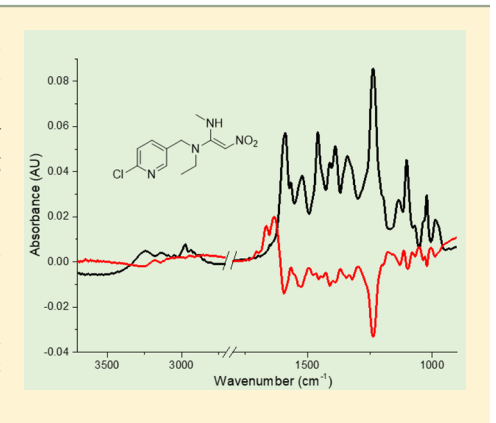
Photochemistry of Solid Films of the Neonicotinoid Nitenpyram

Kifle Z. Aregahegn, Michael J. Ezell, and Barbara J. Finlayson-Pitts*

Department of Chemistry University of California Irvine, California 92697-2025, United States

Supporting Information

ABSTRACT: The environmental fates of nitenpyram (NPM), a widely used neonicotinoid insecticide, are not well-known. A thin solid film of NPM deposited on a germanium attenuated total reflectance (ATR) crystal was exposed to radiation from a low-pressure mercury lamp at 254 nm, or from broadband low pressure mercury photolysis lamps centered at 350 or 313 nm. The loss during photolysis was followed in time using FTIR. The photolysis quantum yields (ϕ) , defined as the number of NPM molecules lost per photon absorbed, were determined to be $(9.4 \pm 1.5) \times 10^{-4}$ at 350 nm, $(1.0 \pm 0.3) \times 10^{-3}$ at 313 nm, and $(1.2 \pm 0.4) \times 10^{-2}$ at 254 nm $(\pm 2\sigma)$. Imines, one with a carbonyl group, were detected as surface-bound products and gaseous N₂O was generated in low (11%) yield. The UV-vis absorption spectra of NPM in water was different from that in acetonitrile, dichloromethane, and methanol, or in a thin solid film. The photolytic lifetime of solid NPM at a solar zenith angle at 35° is calculated to be 36 min, while that for NPM in water is 269 min, assuming that the quantum yield is the



same as in the solid. Thus, there may be a significant sensitivity to the medium for photolytic degradation and the lifetime of NPM in the environment.

■ INTRODUCTION

Neonicotinoids (NN) are relatively new neurotoxic pesticides that have seen expanding use, now representing one-third of the total world insecticide market. 1,2 They selectively bind to the nicotinic acetylcholine receptors to control sucking pests, 1,3-6 and are reported to have relatively low mammalian toxicity, although the data are not definitive. However, their extensive use, 1,2,9 environmental persistence, 1,10-12 residues found in foods and flowers, 9,13-16 impacts on pollinators, 17-27 aquatic organisms, ²⁸ birds, ^{19,29,30} as well as possibly on human health^{8,20,31} and on other nontarget species³² have raised some concerns. As a result of the risks, the use of some NNs has been restricted by the European Union.³³

In the environment, pesticides are exposed to a range of conditions such as humidity, light and oxidants that can cause degradation, leading to a potential decrease in their efficacy and/or formation of products whose toxicity can be different from the parent compound. 34-36 Nitenpyram, N-((6-chloropyridin-3-yl)methyl)-N-ethyl-N'-methyl-2-nitroethene-1,1-diamine, NPM) has a wide range of applications^{1,37} for agricultural³⁸⁻⁴³ and veterinary use, 44-46 for example, for flea control in dogs and cats. 45 It is used as a seed coating 43 and as a soil treatment, becoming translocated throughout the plant. Nitenpyram has two potential geometrical isomers that differ with respect to the relative orientation of the -NH and -NO₂

The E form has the possibility of intramolecular hydrogen bonding between an oxygen of the -NO2 group and the hydrogen of the -NH group, which is seen in the crystal structure, 47 whereas the Z form does not due to the tertiary amine nitrogen. NPM has been detected in a number of vegetable residues, 48 surface and drinking water, 49-51 and in human urine. 52,53

Nitenpyram absorbs light in the actinic region ($\lambda > 290 \text{ nm}$) and hence loss by photolysis is expected to be important in the environment. The goal of this work is to investigate the photochemistry and hence atmospheric stability of NPM. An unexpected impact of water as a solvent on the UV-vis absorption spectrum was observed, which demonstrates the importance of the medium in which NPM exists for its lifetime in the environment. Possible reasons for this and the atmospheric implications are explored.

MATERIALS AND METHODS

A thin layer of NPM was prepared by evaporation from a solution in acetonitrile ACN) on the top surface of a

November 26, 2017 Received: January 15, 2018 Revised: Accepted: January 18, 2018 Published: January 18, 2018

germanium (Ge) attenuated total reflectance (ATR) crystal (Pike Technologies, 45°, 80 mm × 10 mm × 4 mm) to give a coated area of ~ 4 cm². The depth of penetration (d_p) of the evanescent wave through a thin NPM film was calculated⁵⁴ to be $0.15-0.70 \mu m$ over the $4000-860 \text{ cm}^{-1}$ wavelength range. At 1236 cm⁻¹, assigned to the symmetric stretch of the $-NO_2$ group and used to follow the loss of NPM, $d_p = 0.49 \mu m$ based on the assumption of a thin film (see below) and the known indices of refraction of Ge and air. The coated crystal was then placed in a custom-built ATR reaction cell (Supporting Information (SI) Figure S1) described in detail elsewhere.³⁴ The cell has a quartz window through which the sample can be irradiated while either air (Praxair, Ultra Zero) or N2 (Praxair, UHP, 99.999%) flowed over the NPM coating. In a few cases, photolysis was carried out under vacuum as well. Infrared spectra were recorded (Mattson Galaxy 5020 FTIR, 4 cm⁻¹ resolution, 128 scans) before and during irradiation.

Three different low pressure mercury lamps were used to irradiate NPM. The first is a conventional low pressure mercury lamp whose major emission is a line at 254 nm (UVP, CPQ-5851). The second has an organic phosphor coating that gave a broad emission centered at 313 nm (Jelight, 84-2061-2) while the third has an organic phosphor coating whose emission was centered at 350 nm (UVP, D-28865). In the latter two lamps, mercury lines are superimposed on the broad emission from the organic coating, and a Pyrex glass coverslip was used to filter out the mercury lines below 290 nm. SI Figure S2 shows the emission spectra of the lamps. The relative intensities of the lamps were converted to absolute values using photoisomerization of 2-nitrobenzaldehyde (2-NB) to 2-nitrosobenzoic acid as a chemical actinometer s5-58 as described elsewhere.³⁴

The absolute number of molecules in a thin film of NPM for ATR-FTIR measurements was calculated from a calibration curve of the absorbance measured for NPM/acetonitrile solutions of known concentrations over the range of 25-74 mM. Sufficient volumes of the solutions were applied so as to completely cover the ATR crystal to a depth greatly exceeding the depth of penetration of the evanescent wave. The effective thickness (d_e) of the bulk solution that was probed in this case was calculated⁵⁴ using the refractive indices of Ge and acetonitrile to be $d_e = 0.42 \ \mu \text{m}$ at 1236 cm⁻¹. The effective thickness can be used together with the known NPM concentration and area of the crystal to relate the measured absorbance to the number of NPM molecules probed. This relationship was then used for the thin film experiments to estimate the number of NPM on the crystal surface. Using this approach, a typical initial absorbance of 0.08 at 1236 cm⁻¹ was calculated to correspond to 2×10^{17} molecules of NPM. Using the volume of 1272 Å³ for the unit cell of NPM, ⁵⁹ the thickness of an evenly dispersed NPM film was calculated to be 0.07 μ m, corresponding to approximately 90 monolayers. This is significantly less than the depth of penetration, $d_p = 0.49 \mu m$ at 1236 cm⁻¹. Thus, for all experiments, the entire solid film of NPM was interrogated.

To investigate potential solvent effects, UV/vis absorption spectra of NPM in acetonitrile (ACN, Fisher, 99.5%), dichloromethane (DCM, OmniSolv, 99.9%), methanol Omni-Solv, 99.9%) or water (18.2 M Ω -cm) in a quartz cuvette (Crystal Laboratories, 1 mm path length) were recorded using a photodiode array spectrometer (HP 8452A). The average absorption cross sections of NPM in different solvents were calculated from the spectra of known concentrations of NPM over the range of 0.11-0.66 mM. The transmission spectrum of a thin solid film of NPM was obtained by evaporation from an acetonitrile solution onto one side of a calcium fluoride (CaF₂) window (Harrick Sci. Co., 32 × 2 mm) which was mounted on a glass cell such that the NPM was on the inner surface and could be dried in a flow of dry carrier gas (UHP grade). The spectrum of the thin film was found to be similar to that of a solution of NPM in ACN.

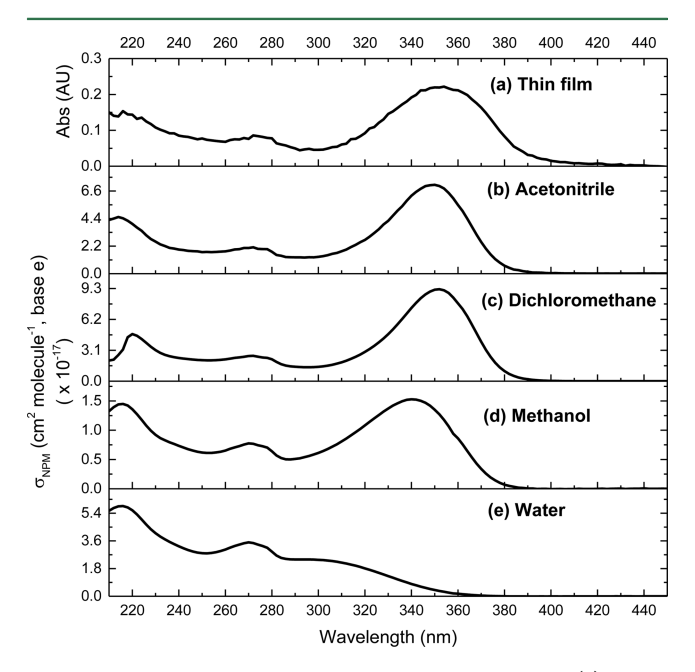


Figure 1. UV-vis absorption spectrum of nitenpyram as (a) a thin solid film in base 10, (b) in acetonitrile, (c) in dichloromethane, (d) in methanol, and (e) in water shown as absorption cross-sections.

To interrogate possible gas phase products, the reaction was carried out in static mode in a closed cell where the cell was positioned in the spectrometer so that the IR beam passed through the ZnSe windows and the gas-phase above the ATR crystal (SI Figure S1). The yield of N₂O was obtained by

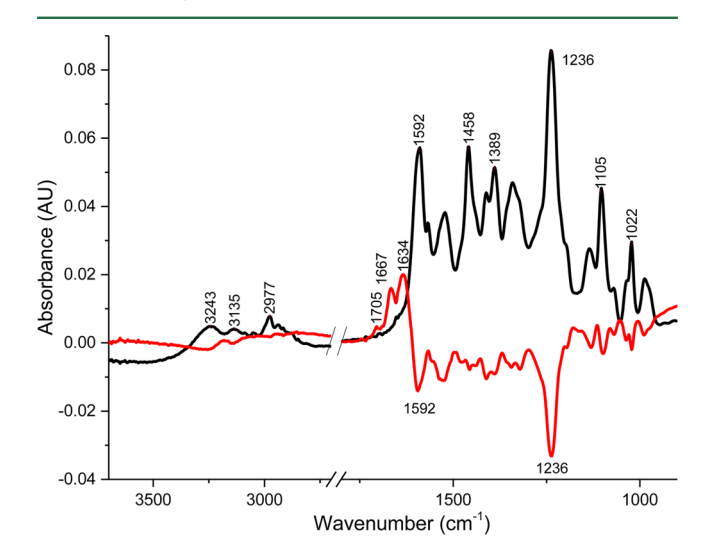


Figure 2. ATR-FTIR spectra of nitenpyram before photolysis (black) and the difference spectrum after 30 min of photolysis using the 350 nm lamp in N₂. The difference spectrum is $log(S_1/S_2)$ where S_1 is the single beam spectrum before photolysis and S_2 is that after photolysis.

Table 1. Measured Photolysis Rate Constants (k_p) and Quantum Yields (ϕ) for Thin Films of Solid Nitenpyram Using Three Different Light Sources

experiment number	photolysis lamp (nm)	carrier gas	$k_{\rm p}~({\rm s}^{-1})$	ϕ
1	254	N_2	1.4×10^{-3}	0.94×10^{-2}
2		N_2	2.0×10^{-3}	1.3×10^{-2}
3		N_2	2.2×10^{-3}	1.4×10^{-2}
4		air	1.8×10^{-3}	1.2×10^{-2}
5		air	1.2×10^{-3}	0.8×10^{-2}
		average $(\pm 2\sigma)^a$	$(1.7 \pm 0.8) \times 10^{-3}$	$(1.2 \pm 0.4) \times 10^{-2}$
1	313	N_2	6.7×10^{-5}	1.0×10^{-3}
2		N_2	5.9×10^{-5}	0.9×10^{-3}
3		N_2	8.4×10^{-5}	1.3×10^{-3}
4		air	5.8×10^{-5}	0.9×10^{-3}
5		air	6.1×10^{-5}	1.0×10^{-3}
		average $(\pm 2\sigma)^a$	$(6.6 \pm 2.1) \times 10^{-5}$	$(1.0 \pm 0.3) \times 10^{-3}$
1	350	N_2	1.5×10^{-4}	9.3×10^{-4}
2		N_2	1.7×10^{-4}	10×10^{-4}
3		air	1.3×10^{-4}	8.2×10^{-4}
4		air	1.6×10^{-4}	9.8×10^{-4}
		average $(\pm 2\sigma)^a$	$(1.5 \pm 0.3) \times 10^{-4}$	$(9.4 \pm 1.5) \times 10^{-4}$

^aErrors do not include possible systematic errors in the absolute light intensity determination, which are estimated to be ~30%.

calibrating the absorbance as a function of known concentrations of gaseous N₂O (Praxair, 99.9%).

Changes in the ATR-FTIR spectrum during photolysis provided data on the solid products formed in the thin film. Further product analysis was carried out using electrospray ionization (ESI) and direct analysis in real time (DART) mass spectrometry, both in the positive ion mode. For both types of mass spectrometry, a drop of NPM in ACN was deposited on a metal screen (stainless steel, 74 Mesh 0.094 mm diameter) and photolyzed in either room air or N2. For ESI-MS, the samples were extracted using a 50/50% (v/v) nanopure water/methanol solvent mixture. In ESI, $[M + H]^+$ and $[M + Na]^+$ are typically the major peaks observed. The ESI ion source operated under a desolvation gas flow of 1000 L h⁻¹, capillary voltage of 3.2 kV, and 500 °C desolvation gas temperature. For DART-MS, the NPM sample on the screen was moved through the DART ionization region to collect the spectra of the unreacted as well as photolyzed samples as described elsewhere. 34 The $[M + H]^+$ peak is the major adduct observed in DART-MS. The DART ion source (DART SVP with Vapur Interface, IonSense, Inc., Saugus, MA) was operated at a gas temperature of 150 °C and a grid electrode voltage of 350 V. Both the ESI and DART ionization systems were interfaced to a mass spectrometer (Xevo TQS, Waters).

Nitenpyram (NPM) was used as received (Sigma-Aldrich, 99.5%). HPLC-ToF-MS (Waters, LCT Premier, isocratic flow mode, calibrated using a PEG standard) of the NPM did not show the presence of detectable amounts of impurities and the exact masses of the $[M + H]^+$ and $[M + Na]^+$ peaks matched those for NPM. NMR (Bruker DRX400) of the NPM was also consistent with the NPM alone. For these analyses, solutions of NPM were prepared by dissolution of the NPM in nanopure water, DCM, methanol or ACN.

RESULTS AND DISCUSSION

Figure 1a shows the absorption spectrum of a thin dry film of NPM formed by evaporation from an ACN solution onto a CaF_2 window. Also shown are absorption spectra in ACN (Figure 1b), dichloromethane (Figure 1c), methanol (Figure 1d), and in water (Figure 1e). The absorption spectrum of the

thin film is similar to that in ACN or dichloromethane, while that in methanol (Figure 1d) is slightly blue-shifted. There is a strong absorption band centered at ~350 nm that has been attributed to a transition involving transfer of electron density to the nitro group from an enamine group. ⁶⁰ Since the actinic cutoff for the troposphere is 290 nm, this strong absorption beyond 290 nm may lead to significant photolysis once released into the atmosphere, if the quantum yields are sufficiently large. In water, however, the spectrum (Figure 1e) is significantly different from the thin film spectrum and from those in the other solvents, with greatly reduced absorption in the 300–350 nm region. As discussed below and shown in the SI, this shift in the spectrum in going from ACN to water is reversible.

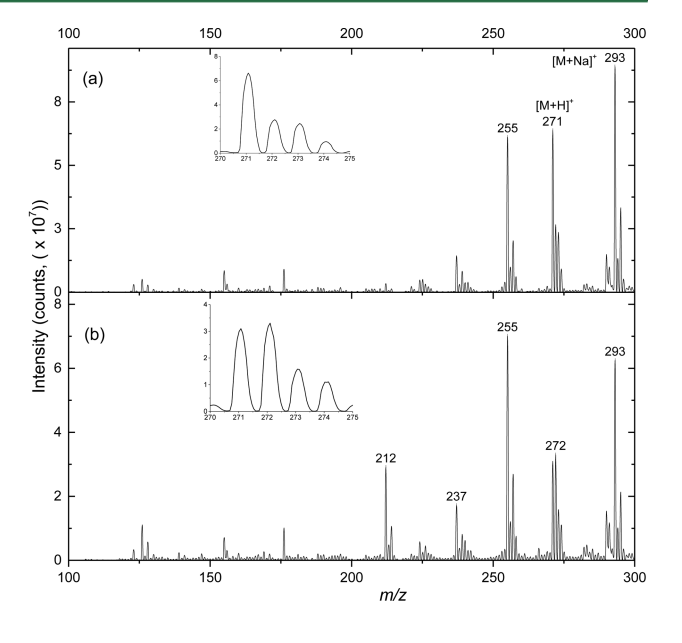
Figure 2 (black line) is the attenuated total reflectance (ATR) infrared spectrum of a thin film of NPM on a Ge ATR crystal, shown as $log(S_0/S_1)$ where S_0 is the single beam of the Ge crystal and S_1 is the crystal with the NPM film before photolysis. Characteristic bands at 1592 and 1236 cm⁻¹ due to asymmetric and symmetric vibrations⁶¹ respectively of the $-NO_2$ group are evident. Peaks in the 2900-3500 cm⁻¹ region are due to C-H and N-H vibrations and those in the 1300-1500 cm⁻¹ region are from a combination of aromatic C=C and C=N vibrational modes.⁶¹ Pyridine ring deformation modes and the aromatic ring-Cl in-plane bending mode are observed at 1022 and 1105 cm⁻¹, respectively. Figure 2 (red line) shows the difference spectrum after 30 min photolysis in N₂ using the 350 nm lamp. Difference spectra are plotted using the initial spectrum before photolysis as the reference, that is, plotted as $log(S_1/S_2)$, where S_2 is the single beam spectrum of the sample after photolysis. Positive peaks thus represent new species and negative peaks the loss of NPM. New peaks due to products in the 1620-1720 cm⁻¹ range are formed. The product spectra were the same for photolysis carried out in air, N_2 or in vacuum. During photolysis using the 350 and 313 nm lamps, the temperature inside the cell was observed to increase up to a maximum of 34 °C. To ensure that loss of NPM and formation of products was not the result of heating, the ATR cell with NPM on the crystal was heated in a separate experiment in the dark up to 50 °C. No loss of NPM or formation of products were observed under these conditions.

Rate constants for decay of NPM (k_n) derived from the slope of first order plots for the loss of NPM using the band at 1236 cm⁻¹ (see SI Figure S3) were used with the absolute lamp emission intensities and the absorption cross sections to obtain quantum yields (ϕ) for photolysis (see eq (I) in SI).³⁴ The quantum yield is defined as the number of NPM molecules lost per photon absorbed. NPM was typically followed out to 30-50% loss to minimize potential complications from overlapping product bands at larger extents of conversion. Quantifying absorption cross sections for the solid film needed to derive the quantum yields was difficult, so that the absorption cross sections of NPM in ACN were used in the calculations. Table 1 summarizes the photolysis rate constants and quantum yields for the three different wavelength regions.

The photolysis rate constant and lifetime at the Earth's surface under tropospheric conditions can be calculated for specific times and locations using the absorption cross sections and quantum yields.⁶² With a quantum yield of 1×10^{-3} , typical of the 313 and 350 nm lamps, the photolysis rate constant for a solar zenith angle of 35° (characteristic of a location at 40° N on April 1) was calculated to be 4.6×10^{-4} s⁻¹, giving a lifetime of NPM under these conditions of 36 min. However, the spectrum in water has greatly reduced absorption around 300 nm (Figure 1e). This is significant for quantifying the loss of NPM in the environment, since nitenpyram has been measured in the aquatic environment and in drinking water from runoff, 50 and the solar intensity increases rapidly from 290 nm to longer wavelengths. 62 Assuming the same quantum yield (1×10^{-3}) as measured for solid NPM, the photolysis rate constant in water at solar zenith angle of 35° was calculated to be 6.2×10^{-5} s⁻¹, corresponding to a lifetime of NPM in aqueous solution of 269 min. This is much longer than the 36 min calculated for the solid. Thus, there may be a significant sensitivity to the medium for photolytic degradation

Photolysis products were further probed using ESI-MS and DART-MS for the solid film products and transmission FTIR for the gas phase. Figure 3a shows the ESI-MS of unreacted NPM and Figure 3b that after photolysis in N₂ using the 350 nm lamp. The MS-MS of the $[M + H]^+$ peak at m/z 271 in the unreacted NPM was similar to that reported by others.⁵⁰ The results were the same for photolysis in air and when using the 254 and 313 nm lamps (although different times were required to reach the same extent of photolysis). Figure 3c,d shows the corresponding DART-MS data. A common feature of both techniques is the formation of [M + H]+, giving a major peak for the unreacted NPM (molar mass 270) at m/z 271. For both ESI and DART, a peak at m/z 212 (and the corresponding³⁷ Cl isotope product) increases significantly with irradiation time, indicating a product with a molecular mass of 211 Da. In DART-MS, there is a large peak at m/z 240 in both the unreacted and photolyzed samples. This is not seen in ESI, but in the latter case, there is a peak at m/z 272 that significantly increases upon photolysis (Figure 3b). The size of this peak relative to that at m/z 271 was somewhat variable from experiment to experiment.

The peak at m/z 212 in the mass spectra and that at 1667 cm⁻¹ in the FTIR spectrum are consistent with the formation of the imine *A*:



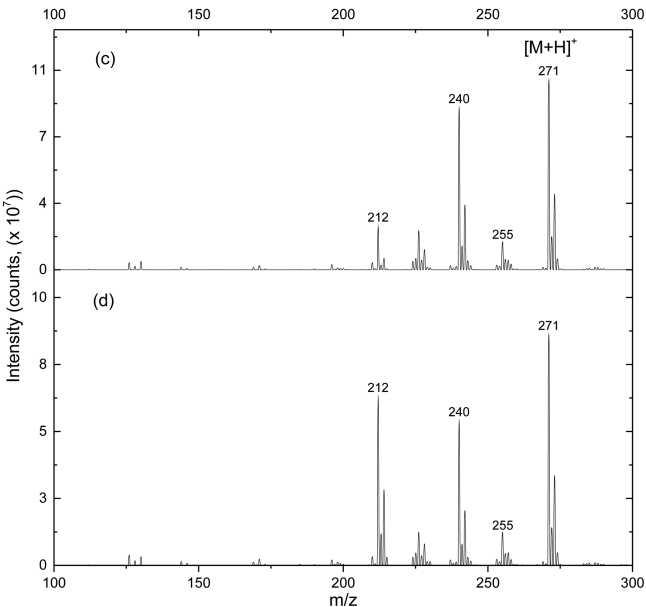


Figure 3. ESI-MS (+) spectra for: (a) nitenpyram before photolysis, and (b) nitenpyram after 3 h of photolysis in N2 using the 350 nm lamp. DART-MS (+) spectra for (c) nitenpyram in dark, and (d) nitenpyram after 3h of photolysis in N₂ using the 350 nm light source.

This is expected to exhibit an $[M + H]^+$ peak at m/z 212, consistent with both the ESI and DART-MS spectra. The infrared peak at 1667 cm⁻¹ (Figure 2) is characteristic of the C=N vibration in imines.⁶¹ This product, *A*, has also been identified as a reaction product of NPM in drinking water.⁵

The ESI-MS spectra also show a peak at m/z 272. MS-MS of this peak gives a fragment at m/z 240. Nizkorodov and coworkers⁶³ have shown that carbonyl compounds can undergo a rapid reaction in methanol solvents to form hemiacetals which

Scheme 1. Proposed Photolysis Mechanism of Nitenpyram

$$\begin{array}{c} N^{H} \stackrel{\circ}{O} \stackrel{h\nu}{N^{+}} \stackrel{\circ}{O} \stackrel{\circ}{O}$$

have molar mass equal to $[M + CH_3OH]$ and appear in ESI at m/z $[M + CH_3OH + H]^+$. We assign the m/z 272 peak to the hemiacetal (RCH(OH)OCH₃) of compound B, which has a molar mass of 239:

In DART-MS, there is a large m/z 240 peak in the dark. Hydroxyl radicals are generated in DART-MS and can react with analytes. It seems likely that the m/z 240 is formed in the DART source itself, and what is formed during the photolysis causes only a small increase relative to what is formed in the source. In the ATR-FTIR spectra, a small peak at 1705 cm⁻¹ (Figure 2) is attributed to formation of a C=O group, consistent with the structure of this compound. The peak at 1634 cm⁻¹ is assigned to the C=N stretch of B, which is redshifted compared to that for A due to the conjugation with the -C=O group.

Transmission FTIR measurements of the gas-phase show production of N_2O (SI Figure S4) identified by comparison to that of an authentic sample. 34 The average molar N_2O yield, defined as $\Delta N_2O/\Delta NPM$, was measured to be 0.11 \pm 0.01 (2σ) at all wavelengths and in air, N_2 or in a few experiments, in vacuum (SI Table S1). The yield is much smaller compared to that from the neonicotinoid imidacloprid, a nitroguanidine, where the yields were within experimental error of unity at 305 nm and $\sim\!\!0.53\pm0.10$ (1σ) at 254 nm. 34

A proposed mechanism that is consistent with the product data is shown in Scheme 1. Under photolysis conditions, the $-\mathrm{NO}_2$ group first isomerizes to an excited nitrite, $-\mathrm{ONO}_3$, which can eliminate HNO to generate the imine aldehyde B. Alternatively, it can eliminate NO and form a resonance stabilized alkoxy radical. 64,65 Given that the NO produced will

be trapped in the solid for some period of time, it has an opportunity to add to the carbon radical site to form the nitroso aldehyde C. This intermediate may decompose via loss of HNO to generate compound B, or eliminate CO to generate an oxime which can isomerize to a nitroso diamine and then decompose to give HNO and an imine of mass 211. Supporting such pathways is the observation of the formation of a carbonyl compound and HNO from the photolysis of alkyl nitrites in low temperature matrices. 64,66 While CO was observed in a few 254 nm photolysis experiments at longer reaction times, the concentrations under most conditions may be under our detection limit (estimated to be 1×10^{14} cm⁻³). The steps in Scheme 1 show short-lived intermediates that connect NPM to the observed products; the fact that the products were the same in air as in N2 suggests the intermediates are not sufficiently long-lived to react with O_2 .

It is well-known that the bimolecular reaction of HNO forms $N_2O.^{67-70}$ This requires that an HNO finds another HNO, which is consistent with the relatively small yield (11%) of $N_2O.$ Given the different imines and aldehydes formed, two peaks in the C=N region of the infrared spectrum (1667 and 1634 cm⁻¹) and one due to -C=O (1705 cm⁻¹) are consistent with this mechanism.

A question remains as to why the spectrum of NPM shows such a dramatic shift in the presence of water. Changing the composition of the solvent from pure ACN to pure water in a stepwise fashion continuously blue-shifted the NPM peak at 350 nm (SI Figure S5). Formation of a thin solid film of NPM on a silicon wafer by evaporation from an ACN solution and then extraction in water gave the same spectrum as NPM in water; similarly, evaporation from a water solution followed by extraction using ACN gave the same spectrum as for NPM in an ACN solution (SI Figure S6). There was a reversible change in the infrared peaks associated with the $-NO_2$ group on exposure of a thin solid film to water followed by drying (SI Figure S7). Thus, the effect of water is reversible, and not due to an irreversible reaction.

Scheme 2. Different Resonance Structures of Nitenpyram

One possible reason for the shift is that that water disrupts the intramolecular hydrogen bonding, possibly converting the more stable E to the Z form. If the $\pi \to \pi^*$ transition in the Z form is increased in energy, a reversible shift to shorter wavelengths would result, consistent with the data. A second possibility is an effect of water on resonance structures of NPM. Shown in Scheme 2 are six reasonable resonance structures for NPM which, taken together, shift electron density toward the nitro chromophore and may explain the observed strong absorption peak at ~350 nm, beyond what is observed for nitro compounds lacking such extensive conjugation. For these structures to fully participate, all the numbered atoms 1 through 6 must be sp² hybridized (or nearly so). Atoms 1 through 4 are indeed sp² hybridized and provide the right geometry for overlapping p-orbitals. Nitrogen atoms 5 and 6 might ordinarily be expected to be sp³ hybridized. However, the increased delocalization energy from extended conjugation should provide the driving force so these N atoms also take on some sp² hybrid character. If there were to be a loss of conjugation when NPM is placed in water, then loss of electron density from the nitro chromophore would explain the observed shift to shorter wavelengths as is observed.

In short, nitenpyram in the troposphere is expected to have a relatively short lifetime. The actual value of the lifetime may depend on whether it is on a surface such as seeds or soil, or in water where the absorption spectrum does not extend as far into the actinic region. Imines, whose toxicity is not known, are formed as products. Thus, whether this photochemistry changes the toxicity to various species compared to the parent NPM remains to be investigated.

ASSOCIATED CONTENT

S Supporting Information

The Supporting Information is available free of charge on the ACS Publications website at DOI: 10.1021/acs.est.7b06011.

Reaction cell schematic, details of the photolysis, quantum yield and N2O measurements, the UV-visible absorption spectra in ACN/water mixtures and the effect of water vapor on a thin NPM film (PDF)

AUTHOR INFORMATION

Corresponding Author

*Phone: (949) 824-7670; fax: (949) 824-2420; e-mail: bjfinlay@uci.edu.

ORCID ®

Barbara J. Finlayson-Pitts: 0000-0003-4650-168X

The authors declare no competing financial interest.

ACKNOWLEDGMENTS

This work was funded by National Science Foundation (Grant # 1404233 and 1707883) and an NSF Major Research Instrumentation (MRI) program (Grant # 1337080). We thank Dr. Felix Grun for helpful discussions and exact mass measurements, and Dr. Phil Dennison for assistance with and helpful discussions on the NMR measurements. We are also grateful to Professor R. Benny Gerber and Dr. Dorit Shemesh for helpful discussions.

REFERENCES

- (1) Simon-Delso, N.; Amaral-Rogers, V.; Belzunces, L. P.; Bonmatin, J. M.; Chagnon, M.; Downs, C.; Furlan, L.; Gibbons, D. W.; Giorio, C.; Girolami, V.; Goulson, D.; Kreutzweiser, D. P.; Krupke, C. H.; Liess, M.; Long, E.; McField, M.; Mineau, P.; Mitchell, E. A. D.; Morrissey, C. A.; Noome, D. A.; Pisa, L.; Settele, J.; Stark, J. D.; Tapparo, A.; Van Dyck, H.; Van Praagh, J.; Van der Sluijs, J. P.; Whitehorn, P. R.; Wiemers, M. Systemic insecticides (neonicotinoids and fipronil): Trends, uses, mode of action and metabolites. Environ. Sci. Pollut. Res. 2015, 22 (1), 5-34.
- (2) Douglas, M. R.; Tooker, J. F. Large-scale deployment of seed treatments has driven rapid increase in use of neonicotinoid insecticides and preemptive pest management in U.S. Field crops. Environ. Sci. Technol. 2015, 49 (8), 5088-5097.
- (3) Jeschke, P.; Nauen, R.; Beck, M. E. Nicotinic acetylcholine receptor agonists: A milestone for modern crop protection. Angew. Chem., Int. Ed. 2013, 52 (36), 9464-9485.
- (4) Talley, T. T.; Harel, M.; Hibbs, R. E.; Radić, Z.; Tomizawa, M.; Casida, J. E.; Taylor, P. Atomic interactions of neonicotinoid agonists with AChBP: Molecular recognition of the distinctive electronegative pharmacophore. Proc. Natl. Acad. Sci. U. S. A. 2008, 105 (21), 7606-
- (5) Goulson, D. Review: An overview of the environmental risks posed by neonicotinoid insecticides. J. Appl. Ecol. 2013, 50 (4), 977-987.

- (6) Casida, J. E. Neonicotinoid metabolism: Compounds, substituents, pathways, enzymes, organisms, and relevance. J. Agric. Food Chem. 2011, 59 (7), 2923-2931.
- (7) Koshlukova, S. E. Imidacloprid Risk Characterization Document: Dietary and Drinking Water Exposure; California Environmental Protection Agency: Sacramento, CA, 2006; pp 1-168.
- (8) Cimino, A. M.; Boyles, A. L.; Thayer, K. A.; Perry, M. J. Effects of neonicotinoid pesticide exposure on human health: A systematic review. Environ. Health Perspect. 2017, 125 (2), 155-162.
- (9) Chen, M.; Tao, L.; McLean, J.; Lu, C. Quantitative analysis of neonicotinoid insecticide residues in foods: Implication for dietary exposures. J. Agric. Food Chem. 2014, 62 (26), 6082-6090.
- (10) Anderson, J. C.; Dubetz, C.; Palace, V. P. Neonicotinoids in the Canadian aquatic environment: A literature review on current use products with a focus on fate, exposure, and biological effects. Sci. Total Environ. 2015, 505, 409-422.
- (11) Bonmatin, J. M.; Giorio, C.; Girolami, V.; Goulson, D.; Kreutzweiser, D. P.; Krupke, C.; Liess, M.; Long, E.; Marzaro, M.; Mitchell, E. A. D.; Noome, D. A.; Simon-Delso, N.; Tapparo, A. Environmental fate and exposure; neonicotinoids and fipronil. Environ. Sci. Pollut. Res. 2015, 22 (1), 35-67.
- (12) Main, A. R.; Headley, J. V.; Peru, K. M.; Michel, N. L.; Cessna, A. J.; Morrissey, C. A. Widespread use and frequent detection of neonicotinoid insecticides in wetlands of canada's prairie pothole region. PLoS One 2014, 9 (3), e92821.
- (13) U.S. Food and Drug Administration. Pesticide monitoring program: Fiscal year 2014 pesticide report. https://www.fda.gov/ downloads/Food/FoodborneIllnessContaminants/Pesticides/ UCM546325.pdfa.Gov/downloads/food/ foodborneillnesscontaminants/pesticides/ucm546325.Pdf (accessed september 2017).
- (14) Mitchell, E. A. D.; Mulhauser, B.; Mulot, M.; Mutabazi, A.; Glauser, G.; Aebi, A. A worldwide survey of neonicotinoids in honey. Science 2017, 358, 109-111.
- (15) Botias, C.; David, A.; Horwood, J.; Abdul-Sada, A.; Nicholls, E.; Hill, E.; Goulson, D. Neonicotinoid residues in wildflowers, a potential route of chronic exposure for bees. Environ. Sci. Technol. 2015, 49 (21), 12731 - 12740
- (16) Botias, C.; David, A.; Horwood, J.; Abdul-Sada, A.; Nicholls, E.; Hill, E.; Goulson, D. Response to comment on "neonicotinoid residues in wildflowers, a potential route of chronic exposure for bees". Environ. Sci. Technol. 2016, 50 (3), 1630-1631.
- (17) Chagnon, M.; Kreutzweiser, D.; Mitchell, E. A. D.; Morrissey, C. A.; Noome, D. A.; Van der Sluijs, J. P. Risks of large-scale use of systemic insecticides to ecosystem functioning and services. Environ. Sci. Pollut. Res. 2015, 22 (1), 119-134.
- (18) Di Prisco, G.; Cavaliere, V.; Annoscia, D.; Varricchio, P.; Caprio, E.; Nazzi, F.; Gargiulo, G.; Pennacchio, F. Neonicotinoid clothianidin adversely affects insect immunity and promotes replication of a viral pathogen in honey bees. Proc. Natl. Acad. Sci. U. S. A. 2013, 110 (46), 18466-18471.
- (19) Doublet, V.; Labarussias, M.; de Miranda, J. R.; Moritz, R. F. A.; Paxton, R. J. Bees under stress: Sublethal doses of a neonicotinoid pesticide and pathogens interact to elevate honey bee mortality across the life cycle. Environ. Microbiol. 2015, 17 (4), 969-983.
- (20) Goulson, D.; Nicholls, E.; Botías, C.; Rotheray, E. L. Bee declines driven by combined stress from parasites, pesticides, and lack of flowers. Science 2015, 347 (6229), 1255957.
- (21) Kessler, S. C.; Tiedeken, E. J.; Simcock, K. L.; Derveau, S.; Mitchell, J.; Softley, S.; Stout, J. C.; Wright, G. A. Bees prefer foods containing neonicotinoid pesticides. Nature 2015, 521 (7550), 74-76.
- (22) Mommaerts, V.; Reynders, S.; Boulet, J.; Besard, L.; Sterk, G.; Smagghe, G. Risk assessment for side-effects of neonicotinoids against bumblebees with and without impairing foraging behavior. Ecotoxicology 2010, 19 (1), 207-215.
- (23) Pisa, L. W.; Amaral-Rogers, V.; Belzunces, L. P.; Bonmatin, J. M.; Downs, C. A.; Goulson, D.; Kreutzweiser, D. P.; Krupke, C.; Liess, M.; McField, M.; Morrissey, C. A.; Noome, D. A.; Settele, J.; Simon-Delso, N.; Stark, J. D.; Van der Sluijs, J. P.; Van Dyck, H.; Wiemers, M.

- Effects of neonicotinoids and fipronil on non-target invertebrates. Environ. Sci. Pollut. Res. 2015, 22 (1), 68-102.
- (24) Raine, N. E.; Gill, R. J. Ecology: Tasteless pesticides affect bees in the field. Nature 2015, 521 (7550), 38-40.
- (25) Rundlof, M.; Andersson, G. K. S.; Bommarco, R.; Fries, I.; Hederstrom, V.; Herbertsson, L.; Jonsson, O.; Klatt, B. K.; Pedersen, T. R.; Yourstone, J.; Smith, H. G. Seed coating with a neonicotinoid insecticide negatively affects wild bees. Nature 2015, 521 (7550), 77-
- (26) Tsvetkov, N.; Samson-Robert, O.; Sood, K.; Patel, H. S.; Malena, D. A.; Gajiwala, P. H.; Maciukiewicz, P.; Fournier, V.; Zayed, A. Chronic exposure to neonicotinoids reduces honey bee health near corn crops. Science 2017, 356 (6345), 1395-1397.
- (27) Stanley, D. A.; Garratt, M. P. D.; Wickens, J. B.; Wickens, V. J.; Potts, S. G.; Raine, N. E. Neonicotinoid pesticide exposure impairs crop pollination services provided by bumblebees. Nature 2015, 528 (7583), 548-552.
- (28) Yan, S.; Wang, J.; Zhu, L.; Chen, A.; Wang, J. Toxic effects of nitenpyram on antioxidant enzyme system and DNA in zebrafish (danio rerio) livers. Ecotoxicol. Environ. Saf. 2015, 122, 54-60.
- (29) Hallmann, C. A.; Foppen, R. P. B.; van Turnhout, C. A. M.; de Kroon, H.; Jongejans, E. Declines in insectivorous birds are associated with high neonicotinoid concentrations. Nature 2014, 511, 341-343.
- (30) Mineau, P.; Palmer, C. The impact of the nation's most widely used insecticides on birds. Am. Bird Conserv. 2013, 1-97.
- (31) Forrester, M. Neonicotinoid insecticide exposures reported to six poison centers in texas. Hum. Exp. Toxicol. 2014, 33 (6), 568-573.
- (32) Gibbons, D.; Morrissey, C.; Mineau, P. A review of the direct and indirect effects of neonicotinoids and fipronil on vertebrate wildlife. Environ. Sci. Pollut. Res. 2015, 22 (1), 103-118.
- (33) European Union, European commission implementing regulation (EU) no 485/2013. J. EU 2013.
- (34) Aregahegn, K. Z.; Shemesh, D.; Gerber, R. B.; Finlayson-Pitts, B. J. Photochemistry of thin solid films of the neonicotinoid imidacloprid on surfaces. Environ. Sci. Technol. 2017, 51 (5), 2660-2668.
- (35) Brown, M. A.; Petreas, M. X.; Okamoto, H. S.; Mischke, T. M.; Stephens, R. D. Monitoring of malathion and its impurities and environmental transformation products on surfaces and in air following an aerial application. Environ. Sci. Technol. 1993, 27 (2), 388 - 397
- (36) Scholz, K.; Reinhard, F. Photolysis of imidacloprid (NTN 33893) on the leaf surface of tomato plants. Pestic. Sci. 1999, 55 (6), 652-654.
- (37) Jeschke, P.; Nauen, R., 5.3 Neonicotinoid insecticides. In Comprehensive Molecular Insect Science; Elsevier: Amsterdam, 2005; pp 53-105.
- (38) Mansoor, M. M.; Raza, A. B. M.; Abbas, N.; Aqueel, M. A.; Afzal, M. Resistance of green lacewing, chrysoperla carnea stephens to nitenpyram: Cross-resistance patterns, mechanism, stability, and realized heritability. Pestic. Biochem. Physiol. 2017, 135, 59-63.
- (39) Wang, S.; Zhang, Y.; Yang, X.; Xie, W.; Wu, Q. Resistance monitoring for eight insecticides on the sweetpotato whitefly (hemiptera: Aleyrodidae) in china. J. Econ. Entomol. 2017, 110 (2), 660-666.
- (40) Wei, Q.; Mu, X.-C.; Yu, H.-Y.; Niu, C.-D.; Wang, L.-X.; Zheng, C.; Chen, Z.; Gao, C.-F. Susceptibility of empoasca vitis (hemiptera: Cicadellidae) populations from the main tea-growing regions of china to thirteen insecticides. Crop Prot. 2017, 96, 204-210.
- (41) Zhang, J.; Hu, L.; Ling, S.; Liu, J.; Chen, H.; Zhang, R. Toxic effects of nitenpyram on the brown planthopper, nilaparvata lugens (stål) (homoptera: Delphacidae). J. Entomol. Sci. 2010, 45 (3), 220-226
- (42) Zhang, J.; Yuan, F.; Liu, J.; Chen, H.; Zhang, R. Sublethal effects of nitenpyram on life-table parameters and wing formation of nilaparvata (Stål) (Homoptera: Delphacidae). Appl. Entomol. Zool. **2010**, 45 (4), 569–574.
- (43) Zhang, Z.; Zhang, X.; Wang, Y.; Zhao, Y.; Lin, J.; Liu, F.; Mu, W. Nitenpyram, dinotefuran, and thiamethoxam used as seed treatments

- act as efficient controls against aphis gossypii via high residues in cotton leaves. *J. Agric. Food Chem.* **2016**, *64* (49), 9276–9285.
- (44) Hovda, L. R.; Hooser, S. B. Toxicology of newer pesticides for use in dogs and cats. *Vet. Clin. North Am. Small Anim. Pract.* **2002**, 32 (2), 455–467.
- (45) Schenker, R.; Tinembart, O.; Humbert-Droz, E.; Cavaliero, T.; Yerly, B. Comparative speed of kill between nitenpyram, fipronil, imidacloprid, selamectin and cythioate against adult ctenocephalides felis (bouche) on cats and dogs. *Vet. Parasitol.* **2003**, *112* (3), 249–254.
- (46) Matsuda, K.; Kanaoka, S.; Akamatsu, M.; Sattelle, D. B. Diverse actions and target-site selectivity of neonicotinoids: Structural insights. *Mol. Pharmacol.* **2009**, 76 (1), 1-10.
- (47) Xu, L. Z.; Yang, Z.; Yi, X.; An, G. W. (E)-N-(6-chloro-3-pyridylmethyl)-N-ethyl-N '-methyl-2-nitroethylene-1,1-diamine. *Acta Crystallogr., Sect. E: Struct. Rep. Online* **2008**, *64*, O1074–U2154.
- (48) Obana, H.; Okihashi, M.; Akutsu, K.; Kitagawa, Y.; Hori, S. Determination of acetamiprid, imidacloprid, and nitenpyram residues in vegetables and fruits by high-performance liquid chromatography with diode-array detection. *J. Agric. Food Chem.* **2002**, *50* (16), 4464–4467
- (49) Dong, X.; Jiang, D.; Liu, Q.; Han, E.; Zhang, X.; Guan, X.; Wang, K.; Qiu, B. Enhanced amperometric sensing for direct detection of nitenpyram via synergistic effect of copper nanoparticles and nitrogen-doped graphene. *J. Electroanal. Chem.* **2014**, 734, 25–30.
- (50) Noestheden, M.; Roberts, S.; Hao, C. Nitenpyram degradation in finished drinking water. *Rapid Commun. Mass Spectrom.* **2016**, 30 (13), 1653–1661.
- (51) Morrissey, C. A.; Mineau, P.; Devries, J. H.; Sanchez-Bayo, F.; Liess, M.; Cavallaro, M. C.; Liber, K. Neonicotinoid contamination of global surface waters and associated risk to aquatic invertebrates: A review. *Environ. Int.* **2015**, *74*, 291–303.
- (52) Osaka, A.; Ueyam, J.; Kondo, T.; Nomura, H.; Sugiura, Y.; Saito, I.; koNakane, K.; Takaishi, A.; Ogi, H.; Wakusawa, S.; YukiIto; Kamijima, M. Exposure characterization of three major insecticide lines in urine of young children in Japan—neonicotinoids, organophosphates, and pyrethroids. *Environ. Res.* **2016**, *147*, 89–96.
- (53) Ueyama, J.; Nomura, H.; Kondo, T.; Saito, I.; Ito, Y.; Osaka, A.; Kamijima, M. Biological monitoring method for urinary neonicotinoid insecticides using LC-MS/MS and its application to Japanese adults. *J. Occup. Health* **2014**, *56* (6), 461–468.
- (54) Harrick, N. J. Internal Reflection Spectroscopy; Interscience Publishers: New York, NY, 1967; p 327.
- (55) Allen, J. M.; Allen, S. K.; Baertschi, S. W. 2-nitrobenzaldehyde: A convenientUV-A and UV-B chemical actinometer for drug photostability testing. *J. Pharm. Biomed. Anal.* **2000**, 24 (2), 167–178.
- (56) Leighton, P. A.; Lucy, F. A. The photoisomerization of the onitrobenzaldehydes I. Photochemical results. *J. Chem. Phys.* **1934**, 2 (11), 756–759.
- (57) Pitts, J. N.; Wan, J. K. S.; Schuck, E. A. Photochemical studies in an alkali halide matrix. I. An *o*-nitrobenzaldehyde actinometer and its application to a kinetic study of the photoreduction of benzophenone by benzhydrol in a pressed potassium bromide disk. *J. Am. Chem. Soc.* **1964**, *86* (18), 3606–3610.
- (58) Vichutinskaya, Y. V.; Postnikov, L. M.; Kushnerev, M. Y. The use of o-nitrobenzaldehyde as internal actinometer when studying photo-oxidative breakdown of thin unoriented polycaprolactam films. *Polym. Sci. U.S.S.R.* 1975, *17* (3), 716–721.
- (59) Xu, L.-Z.; Yang, Z.; Xu, Y.; Ana, G. W. (E)-N-(6-chloro-3-pyridylmethyl)-N-ethyl-N'-methyl-2-nitroethylene-1,1-diamine. *Acta Crystallogr., Sect. E: Struct. Rep. Online* **2008**, *E64*, 01074.
- (60) Kleier, D.; Holden, I.; Casida, J. E.; Ruzo, L. O. Novel photoreactions of an insecticidal nitromethylene heterocycle. *J. Agric. Food Chem.* **1985**, 33 (5), 998–1000.
- (61) Socrates, G. Infrared and Raman Characteristic Group Frequencies, 3rd ed.; Wiley: New York, 2004.
- (62) Finlayson-Pitts, B. J.; Pitts, J. N. Chemistry of the Upper and Lower Atmosphere: Theory, Experiments, and Applications; Academic Press: San Diego, 2000; p xxii, 969 p.

- (63) Bateman, A. P.; Walser, M. L.; Desyaterik, Y.; Laskin, J.; Laskin, A.; Nizkorodov, S. A. The effect of solvent on the analysis of secondary organic aerosol using electrospray ionization mass spectrometry. *Environ. Sci. Technol.* **2008**, 42 (19), 7341–7346.
- (64) Calvert, J. G.; Pitts, J. N. J. *Photochemistry*; John Wiley & Sons: New York, 1966.
- (65) Kan, R. O. Organic Photochemistry; McGraw-Hill: New York, 1966.
- (66) Brown, H. W.; Pimentel, G. C. Photolysis of nitromethane and of methyl nitrite in an argon matrix infrared detection of nitroxyl, HNO. *J. Chem. Phys.* **1958**, 29 (4), 883–888.
- (67) Bryukov, M. G.; Kachanov, A. A.; Timonnen, R.; Seetula, J.; Vandoren, J.; Sarkisov, O. M. Kinetics of HNO reactions with O₂ and HNO. *Chem. Phys. Lett.* **1993**, 208 (5–6), 392–398.
- (68) Callear, A. B.; Carr, R. W. Thermal-decomposition of HNO. J. Chem. Soc., Faraday Trans. 2 1975, 71, 1603–1609.
- (69) Lin, M. C.; He, Y. S.; Melius, C. F. Theoretical interpretation of the kinetics and mechanisms of the HNO + HNO and HNO + 2NO reactions with a unified model. *Int. J. Chem. Kinet.* **1992**, *24* (5), 489–516.
- (70) Luttke, W.; Skancke, P. N.; Traetteberg, M. On the dimerization process of nitroso-compounds a theoretical-study of the reaction 2 HNO (HNO)₂. *Theor. Chim. Acta* **1994**, 87 (4–5), 321–333.